DMD Fast Forward. Published on September 1, 2015 as DOI: 10.1124/dmd.115.064790
This article has not been copyedited and formatted. The final version may differ from this version.

DMD/2015/064790

In vitro characterization of the human liver microsomal kinetics and reaction phenotyping of olanzapine metabolism

Porntipa Korprasertthaworn, Thomas M Polasek, Michael J Sorich, Andrew J McLachlan, John O Miners, Geoffrey T Tucker, and Andrew Rowland

Department of Clinical Pharmacology and Flinders Centre for Innovation in Cancer, Flinders University School of Medicine, Adelaide, Australia (PK, TMP, MJS, JOM, AR)

Department of Pharmacology, Faculty of Science, Mahidol University, Bangkok, Thailand (PK)

Faculty of Pharmacy, University of Sydney, Sydney, Australia (AJM)

University of Sheffield (Emeritus), Sheffield, United Kingdom (GTT)

Running title: *In vitro* characterization of olanzapine metabolism

Corresponding author:

Dr Andrew Rowland

Department of Clinical Pharmacology

Flinders University School of Medicine

Flinders Medical Centre

Bedford Park

SA 5042

Australia

Telephone 61-8-8204 7546

Fax 61-8-8204 5114

Email andrew.rowland@flinders.edu.au

Manuscript details:

Number of text pages (including references and legends) – 36

Number of tables – 4

Number of figures – 5

Number of references – 43

Abstract – 206 words

Introduction – 759 words

Discussion – 1,331 words

Abbreviations:

BSA, albumin from bovine serum; CPR, NADPH cytochrome P450 oxidoreductase; CYP, cytochrome P450; FMO, flavin-containing monooxygenase; HEK293T, human embryonic kidney 293T cell line; HLM, human liver microsome; m/z, mass-to-charge ratio; OLZ, olanzapine; rCYP, recombinant cytochrome P450; rUGT, recombinant UDP-glucuronosyltransferase; UGT, UDP-glucuronosyltransferase; UPLC-MS, ultra-performance liquid chromatography-mass spectrometry

Abstract

Olanzapine (OLZ) is an atypical antipsychotic used in the treatment of schizophrenia and related psychoses. The metabolism of OLZ is complex and incompletely characterized. The aim of this study was to elucidate the enzymes and pathways involved in the metabolism of OLZ and to determine the kinetics of OLZ oxidation and glucuronidation by human liver microsomes (HLMs), and recombinant cytochrome P450 (rCYP) and recombinant UDP-glucuronosyltransferase (rUGT) enzymes. A UPLC-MS method was developed and validated to quantify OLZ, its four oxidative metabolites (*N*-desmethyl-OLZ, 2-hydroxymethyl-OLZ, 7-hydroxy-OLZ and OLZ-*N*-oxide), and two *N*-glucuronides (OLZ-10-*N*-glucuronide and OLZ-4′-*N*-glucuronide). Consistent with previous reports, UGT1A4, CYP1A2 and flavin-containing monooxygenase 3 play major roles in catalyzing the formation of OLZ-10-*N*-glucuronide, 7-hydroxy-OLZ and OLZ-*N*-oxide, respectively. In addition, a previously uncharacterized major contribution of CYP2C8 to OLZ-*N*-demethylation was demonstrated. The kinetics of OLZ metabolite formation (K_m and V_{max}) by HLMs, rCYP and rUGT enzymes were characterized in the presence of bovine serum albumin (BSA; 2% w/v). Consistent with the known effect of BSA on CYP1A2, CYP2C8 and UGT1A4 activities, K_m values reported here are lower than previously reported values for OLZ metabolic pathways. In addition to CYP1A2-mediated OLZ-*N*-demethylation, these results suggest that other CYP enzymes, particularly CYP2C8, contribute significantly to oxidative OLZ metabolism through catalysis of OLZ-*N*-demethylation.

Introduction

Olanzapine (OLZ) is an atypical antipsychotic indicated for the treatment of schizophrenia and related psychoses (Rosenheck et al., 2003). While OLZ is effective for the acute management of psychosis, up to 80% of patients discontinue treatment within five years due to either a lack of long term efficacy or drug-related adverse events (Schwenger et al., 2011). In this regard, plasma OLZ and metabolite (primarily *N*-desmethyl-OLZ) concentrations have been identified as important markers of both clinical response to OLZ and the occurrence of adverse effects such as weight gain, hyperinsulinemia and hyperlipidemia (Perry et al., 2001; Mauri et al., 2007; Nozawa et al., 2008). Accordingly, therapeutic drug monitoring (TDM) for OLZ is recommended in a number of clinical guidelines and a therapeutic concentration range of 20 to 80 µg/L has been established (Baumann et al., 2004).

OLZ is cleared primarily via hepatic metabolism, with <10% of the drug excreted unchanged in urine. The metabolism of OLZ is complex, involving multiple pathways and drug metabolizing enzyme families (Figure 1). Consistent with their roles in the metabolism of a myriad of drugs (Miners and Mackenzie 1991; Zanger and Schwab 2013; Rowland et al., 2013), available evidence indicates that members of the cytochrome P450 (CYP) and UDP-glucuronosyltransferase (UGT) superfamilies are extensively involved in the oxidative and conjugative metabolism of OLZ, respectively, with a minor contribution from the flavin-containing monooxygenase (FMO) enzymes (Ring et al., 1996; Linnet K, 2002). The major primary metabolites of OLZ formed in humans are *N*-desmethyl-OLZ, OLZ-10-*N*-glucuronide, 2-hydroxymethyl-OLZ and OLZ-*N*-oxide (Kassahun et al., 1997). Although not detected *in vivo*, formation of 7-hydroxy-OLZ has been reported *in vitro* with human liver microsomes (HLM) as the enzyme source (Ring et al., 1996). Despite the established relationship between plasma *N*-desmethyl-OLZ concentration and clinical outcomes, there has been only one study that has evaluated the oxidative pathways of OLZ in a systematic manner (Ring et al., 1996). Current data suggest that CYP 1A2, 2C9, 2D6, 2E1 and 3A4 and FMO3 contribute to the oxidative metabolism of OLZ. CYP1A2 has been identified as the major enzyme responsible for the formation of *N*-desmethyl-OLZ and 7-hydroxy-OLZ, while CYP2D6 has been identified as the major enzyme responsible for 2-hydroxymethyl-OLZ formation (Ring et al., 1996). However, the roles of additional hepatic drug

metabolizing CYP enzymes, particularly CYP 2B6, 2C8 and 2C19, in the oxidative metabolism of OLZ remains poorly characterized. Notably, when considering data presented by Ring et al. (1996), the identity of CYP enzymes involved in OLZ oxidative metabolism were primarily assigned using HLM as the enzyme source and on the basis of surrogate markers, i.e. correlations with immunoquantified enzyme levels and enzyme-selective catalytic activities.

Given the purported major role of CYP1A2 in the formation of *N*-desmethyl-OLZ, a number of studies have attempted to correlate CYP1A2 phenotype and genotype with plasma OLZ and metabolite concentrations (Hägg et al., 2001; Carrillo et al., 2003; Shirley et al., 2003, Nozawa et al., 2008, Laika et al., 2010, Ghotbi et al., 2010, Skogh et al., 2011, Söderberg et al., 2013a). While studies have demonstrated moderate correlations with end-points such as OLZ oral clearance (Carrillo et al., 2003, Shirley et al., 2003), these reports have consistently demonstrated a lack of correlation between CYP1A2 phenotype or genotype and plasma OLZ metabolite concentrations. Taken together, these data support the hypothesis that other CYP enzymes play a clinically important role in the metabolism of OLZ, particularly the formation of *N*-desmethyl-OLZ. Given the importance of *N*-desmethyl-OLZ concentrations as a marker of clinical outcomes, clarification of the identity of the CYP enzymes involved in this OLZ metabolic pathway is warranted.

Thus, the current study sought to re-evaluate the metabolic pathways involved in OLZ clearance using ultra-performance liquid chromatography-mass spectrometry (UPLC-MS) for metabolite quantification and accounting for recently identified potential confounding factors associated with *in vitro* drug kinetic studies, notably non-specific binding of substrate (McLure et al., 2000; Rowland et al., 2007 and 2008a; Wattanachai et al., 2011 and 2012) and inhibition of selected CYP and UGT enzymes by long-chain unsaturated fatty acids released from membranes during the course of an incubation (Tsoutsikos et al., 2004; Yao et al., 2006; Rowland et al., 2008 a and b). Data confirmed the role of FMO3 in the formation of OLZ-*N*-oxide but excluded a significant role of this enzyme in the formation of other OLZ metabolites. Kinetic analyses were performed to characterize the CYP catalyzed OLZ oxidative pathways and OLZ glucuronidation pathways using both HLMs and

DMD Fast Forward. Published on September 1, 2015 as DOI: 10.1124/dmd.115.064790
This article has not been copyedited and formatted. The final version may differ from this version.

recombinant enzymes. Kinetic data demonstrate that in addition to CYP1A2 other CYP enzymes, most notably CYP2C8, catalyze the formation of *N*-desmethyl-OLZ at a comparable rate.

Materials and Methods

Materials

2-Hydroxymethyl-OLZ, 2-hydroxymethyl-OLZ-d_3, *N*-desmethyl-OLZ, *N*-desmethyl-OLZ-d_8, OLZ, OLZ-d_3, OLZ-d_3-*N*-oxide and OLZ-*N*-oxide were purchased from Toronto Research Chemicals (North York, ON); ticlopidine from LKT Laboratories (St. Paul, MN); montelukast from Cayman Chemical (Ann Arbor, MI), and BSA (essentially fatty acid free), CYP3cide, D-glucose-6-phosphate disodium salt hydrate, diethyldithiocarbamic acid, furafylline, glucose-6-phosphate dehydrogenase, hecogenin, NADP, quinidine, sulfaphenazole, ticlopidine, tranylcypromine, troleandomycin and UDP-GlcUA from Sigma-Aldrich (St. Louis, MO). Human UGT 2B4, 2B7, 2B10, 2B15 and 2B17 and FMO3 Supersomes were purchased from BD Biosciences (Woburn, MA). All other reagents and solvents were of analytical reagent grade or higher.

Preparation of HLMs and Expression of Recombinant CYPs and UGTs

Human livers (H7, H10, H12, H13 and H40) were obtained from the human liver bank of the Department of Clinical Pharmacology, Flinders University School of Medicine. Approval was obtained from the Flinders Medical Centre Research Ethics Committee for the use of human liver tissue in xenobiotic metabolism studies. Microsomes were prepared by differential centrifugation, as described by Bowalgaha et al. (2005).

Recombinant CYP 1A1, 1A2, 2B6, 2C8, 2C9, 2E1, 3A4 and NADPH cytochrome P450 oxidoreductase (CPR) were co-expressed in *Escherichia coli (E. coli)* according to the general procedure of Boye et al. (2004). The CYP/CPR ratios were close to unity. cDNAs encoding UGT 1A1, 1A3, 1A4, 1A6, 1A7, 1A8, 1A9 and 1A10 were stably expressed in a human embryonic kidney cell line (HEK293T), as described previously (Uchaipichat et al., 2004). Activity of these recombinant UGTs (except UGT1A4) was confirmed using the non-selective substrate 4-methylumbelliferone (Uchaipichat et al., 2004). The activity of UGT1A4 was confirmed using lamotrigine as substrate (Rowland et al., 2006).

DMD Fast Forward. Published on September 1, 2015 as DOI: 10.1124/dmd.115.064790
This article has not been copyedited and formatted. The final version may differ from this version.

OLZ Oxidative Metabolism Assay

Incubations, in a total volume of 200 µL, contained phosphate buffer (1 mM, pH 7.4), HLM (0.5 mg/mL) and OLZ (5 – 400 µM). Following a 5-min pre-incubation, reactions were initiated by the addition of a NADPH-generating system (1 mM NADP, 10 mM glucose-6-phosphate, 2 IU/mL glucose-6-phosphate dehydrogenase and 5 mM $MgCl_2$). Incubations were performed at 37°C in a shaking water bath for 60 min. Reactions were terminated by the addition of ice-cold methanol containing 4% acetic acid (200 µL) and cooling on ice. Samples were subsequently centrifuged at 5000*g* for 10 min at 10°C and a 150 µL aliquot of the resultant supernatant fraction was diluted in 350 µL of mobile phase containing deuterated internal standards (OLZ-d_3, *N*-desmethyl-OLZ-d_8, 2-hydroxymethyl-OLZ-d_3 and OLZ-d_3-*N*-oxide; 25 nM). A 7.5-µL aliquot was injected directly onto the UPLC column.

For reactions performed using recombinant CYP (rCYP) enzymes, incubation mixtures contained CYP protein expressed in *E. coli* membranes in place of HLM protein. Screening experiments were initially performed to assess the capacity of individually expressed rCYP to catalyze the oxidative metabolism of OLZ. These experiments were performed at a rCYP concentration of 25 pmol P450/mL and OLZ concentrations of 50 and 300 µM, with samples incubated for 2 h at 37°C in a shaking water bath. Incubation conditions for subsequent kinetic studies with rCYP were as described above for HLM with the following amendments: rCYP content (10 pmol P450/mL), OLZ (5 – 1000 µM) and incubation time (60 and 10 min for rCYP 1A2 and 2C8, respectively). BSA (2% w/v) was included in all experiments (HLM and rCYP) performed to assess the kinetics of CYP 1A2 and 2C8 catalyzed reactions. Control samples were incubated in the absence of NADPH-generating system and/or protein. Rates of product formation were optimized for linearity with respect to protein concentration and incubation time.

DMD Fast Forward. Published on September 1, 2015 as DOI: 10.1124/dmd.115.064790
This article has not been copyedited and formatted. The final version may differ from this version.

OLZ Glucuronidation Assay

Incubations, in a total volume 200 µL, contained phosphate buffer (1 mM, pH 7.4), $MgCl_2$ (4 mM), HLM (0.25 mg/mL) and OLZ (50 – 1500 µM). HLMs were fully activated by the addition of the pore-forming polypeptide alamethicin (50 µg/mg of protein) with incubation on ice for 30 min (Boase and Miners, 2002). Following a 5-min pre-incubation, reactions were initiated by the addition of UDP-GlcUA (5 mM). Incubations were performed at 37°C in a shaking water bath for 45 min. Reactions were terminated by the addition of ice-cold methanol containing 4% acetic acid (200 µL) and cooling on ice. Samples were subsequently centrifuged at 5000*g* for 10 min at 10°C and a 150 µL aliquot of the resultant supernatant fraction was diluted in 350 µL of mobile phase containing a deuterated OLZ-d_3 internal standard (25 nM). A 7.5-µL aliquot was injected directly onto the UPLC column.

For reactions performed using recombinant human UGTs, incubation mixtures contained UGT1A enzymes expressed in HEK293T cells (as lysate) or UGT2B enzymes expressed in Supersomes. Screening experiments were initially performed to assess the capacity of individually expressed rUGT to glucuronidate OLZ. These experiments were performed at a rUGT concentration of 1 mg/mL and OLZ concentrations of 350 and 1500 µM, with samples incubated for 2 h at 37°C in a shaking water bath. Incubation conditions for subsequent kinetic studies with rUGT were as described above for HLM with the following amendments: rUGT content (0.5 mg/mL) and incubation time 30 min. For the experiments performed in the presence of BSA, reactions were terminated by the addition of ice-cold methanol containing 4% acetic acid (400 µL) and cooling on ice. Control samples were incubated in the absence of UDP-GlcUA and/or protein. The rate of product formation was optimized for linearity with respect to protein concentration and incubation time.

Inhibition Experiments

The effects of CYP enzyme selective inhibitors on the formation of the oxidative metabolites of OLZ were investigated using pooled HLMs as the enzyme source. Furafylline (10 µM), tranylcypromine (1

μM), ticlopidine (3 μM), montelukast (0.2 μM), sulfaphenazole (2.5 μM), quinidine (1 μM), diethyldithiocarbamic acid (10 μM) and CYP3cide (1.5 μM) were used as selective inhibitors of CYP 1A2, 2A6, 2B6/2C19, 2C8, 2C9, 2D6, 2E1 and 3A4, respectively, while hecogenin (10 μM) was used as a selective UGT1A4 inhibitor. Pooled HLMs (0.5 mg/mL) were incubated with 50 μM OLZ in the absence and presence of the selective inhibitors. When required, inhibitors were dissolved in either 50% acetonitrile (CYP3cide) or methanol (furafylline, montelukast and sulfaphenazole) and added to incubations such that the final solvent concentration was either 0.5 or 1% w/v. Control samples were prepared without inhibitors but with an equivalent concentration of solvent. Since furafylline, ticlopidine, diethyldithiocarbamic acid and CYP3cide are mechanism-based inhibitors, pooled HLM proteins were pre-incubated with these compounds in the presence of the NADPH-generating system for 30 min prior to the addition of OLZ. Reaction mixtures were incubated at 37°C for 1 h in a shaking water bath and then terminated and further prepared for analysis as described in oxidative metabolism assay. Percentage inhibition of metabolite formation by enzyme-specific inhibitors was calculated by comparing activity with control activity (without inhibitor) (n=4).

Separation of Olanzapine Metabolites

Chromatographic separations were performed on a Waters ACQUITY^{TM} BEH C18 analytical column (100mm x 2.1mm, 1.7μm; Waters Corp., Milford, MA) using a Waters ACQUITY Ultra Performance LC^{TM} (UPLC) system. The column temperature was maintained at 40°C, while the sample compartment was maintained at 15°C. Analytes were separated by gradient elution at a flow rate of 0.2mL/min. Initial conditions were 87% ammonium formate (10mM, pH 3.0; mobile phase A) and 13% acetonitrile (mobile phase B). The proportion of mobile phase B was increased linearly to 70% over 7min and held for 0.5min. The total run time, including reconditioning of the column to initial conditions, was 9min. Retention times of 2-hydroxymethyl-OLZ, 7-hydroxy-OLZ, *N*-desmethyl-OLZ, OLZ-*N*-oxide, OLZ-10-*N*-glucuronide (2 peaks) and OLZ-4′-*N*-glucuronide under these conditions were 1.7, 2.2, 3.4, 3.8, 1.4, 1.8 and 3.5 min, respectively (Figure 2).

Quantification of Olanzapine Metabolites

Column elutant was monitored by mass spectrometry, performed on a Waters Q-ToF Premier™ quadrupole, orthogonal acceleration time-of-flight tandem mass spectrometer (Q-ToF-MS) operated in positive ion mode with electrospray ionization (ESI+). Instrument acquisition settings are described in Table 1. Time-of-flight (ToF) data were collected in wide pass (MS) mode, with the resolving quadrupole acquiring data between m/z 100 and 650. Selected ion data was extracted at precursor m/z of 299.14 (*N*-desmethyl-OLZ), 329.15 (2-hydroxymethyl-OLZ, 7-hydroxy-OLZ and OLZ-*N*-oxide) and 489.18 (OLZ-10-*N*-glucuronide and OLZ-4′-*N*-glucuronide). Resulting pseudo multiple reaction monitoring (MRM) spectra were analyzed using Waters QuanLynx™ software (Waters Corporation, Sydney, Australia). Quantification of analytes in incubation samples was accomplished by comparison of peak areas with those of authentic standards for each metabolite (25 – 500 nM) with the exception of 7-hydroxy-OLZ and OLZ-10-*N*-glucuronide, which were measured by comparison of peaks to those of the respective external standards 2-hydroxymethyl-OLZ and OLZ.

Binding of OLZ to BSA, HLMs, rCYPs and rUGTs

Binding of OLZ to HLMs, rCYPs, rUGTs and BSA in each enzyme source was measured by equilibrium dialysis according to the method of McLure et al. (2000). The experiments were performed using a Dianorm equilibrium dialysis apparatus consisting of Teflon dialysis cells (capacity of 1.2 mL/side) separated by a Sigma-Aldrich dialysis membrane (molecular mass cut off, 12 kDa). One side of the dialysis cell was loaded with 1 mL of OLZ (10 – 100 µM) in phosphate buffer (1 mM, pH 7.4). The other compartment was loaded with 1 mL of HLMs, rCYPs, rUGTs or a combination of BSA with each enzyme source in phosphate buffer (1 mM, pH 7.4). The dialysis cell assembly was immersed in a water bath maintained at 37°C and rotated at 12 rpm for 4 h. Control experiments were also performed with phosphate buffer or BSA on both sides of the dialysis cells at low and high concentrations of OLZ to ensure that equilibrium was attained. A 200-µL aliquot was collected from each compartment, treated with ice-cold methanol containing 4% acetic acid (400 µL) and cooling on ice. Samples were subsequently centrifuged at 5000*g* for 10 min at 10°C and a 5-µL aliquot of the supernatant fraction was analyzed by high performance liquid chromatography.

DMD Fast Forward. Published on September 1, 2015 as DOI: 10.1124/dmd.115.064790
This article has not been copyedited and formatted. The final version may differ from this version.

Quantification of OLZ Binding

Separation of OLZ was achieved on an Agilent Zorbax Eclipse XDB-C8 column (4.6 × 150 mm, 5 µm; Agilent Technologies, Santa Clara, CA) using a mobile phase comprising 90% 10 mM ammonium formate (pH 3.0) and 10% acetonitrile, at a flow rate of 1 mL/min. The column eluent was monitored at 257 nm. The retention time of OLZ was 3.1 min. OLZ concentrations in dialysis samples were determined by comparison of peak areas with those of an OLZ standard (concentration range of 10 - 100 µM).

Kinetic Analysis

Data points represent the mean of duplicate (< 10% variance) or quadruplicate measurements. Kinetic constants for OLZ oxidative metabolism and glucuronidation were obtained by fitting Michaelis-Menten, substrate inhibition, or Hill equations (see below) to the experimental data using EnzFitter version 2.0 (Biosoft, Cambridge). Goodness of fit was assessed by comparison of the *F* statistic, coefficient of determination (r^2), S.E. of the parameter fit and 95% confidence intervals.

Michaelis-Menten equation:

$$v = \frac{V_{max} \times [S]}{K_m + [S]} \qquad \text{Equation 1}$$

Where v is the rate of reaction, V_{max} is the maximum velocity, K_m is the Michaelis-Menten constant (substrate concentration at 0.5 V_{max}) and [S] is the substrate concentration.

The Hill equation, which describes positive or negative cooperative kinetics:

$$v = \frac{V_{max} \times [S]^n}{S_{50}^n + [S]^n} \qquad \text{Equation 2}$$

Where S_{50} is the substrate concentration resulting in 50% of V_{max} (analogous to K_m in the previous equations) and n is the Hill coefficient.

Substrate inhibition equation:

$$v = \frac{V_{max}}{1 + \frac{K_m}{[S]} + \frac{[S]}{K_{si}}} \qquad \text{Equation 3}$$

Where K_{si} is the constant describing the substrate inhibition reaction.

DMD Fast Forward. Published on September 1, 2015 as DOI: 10.1124/dmd.115.064790
This article has not been copyedited and formatted. The final version may differ from this version.

Results

Binding of OLZ to HLMs, rCYPs, rUGTs and BSA

It has been reported that the *in vitro* activities of certain CYP (particularly 1A2, 2C8 and 2C9) and UGT (particularly 1A9 and 2B7) enzymes are inhibited by long-chain unsaturated fatty acids released from the microsomal membrane during incubations. This inhibition largely manifests as an increase in K_m values (with occasional effects on V_{max}) and hence CL_{int} for the added substrate, which results in an under-prediction of the *in vitro* intrinsic clearance of the substrate (Tsoutsikos et al., 2004; Rowland et al., 2007; 2008a and b; Wattanachai et al., 2011; 2012). In addition, it has been shown that the inhibitory effect of fatty acids can be overcome by sequestration with BSA (Rowland et al., 2007; 2008a; Wattanachai et al., 2012). Thus BSA (2% w/v) was included in incubations for the kinetic experiments performed in this study. However, since the effect of BSA on the kinetics of UGT1A4 catalyzed glucuronidation is less well-characterized, the kinetics of OLZ-10-*N*-glucuronidation were determined in the absence and presence of albumin.

Accordingly, the binding of OLZ to HLMs, *E. coli* membrane (used to express rCYP enzymes) and HEK293T cell lysate (used to express rUGT enzymes) and BSA (2% w/v) was determined by equilibrium dialysis. The extent of OLZ binding was calculated as the concentration of drug in the buffer compartment divided by the concentration of drug in the protein compartment and expressed as a fraction unbound in the incubation mixture ($f_{u,inc}$). The binding of OLZ to HLMs, *E. coli* membrane and HEK293T cell lysate was negligible (<15%) across the OLZ concentration range investigated (10 – 100 µM). However, OLZ did bind significantly to mixtures of HLM and BSA with a mean (± S.D.) $f_{u,inc}$ value of 0.69 ± 0.01. Thus, the concentration of OLZ present in reaction mixtures was corrected for binding in the calculation of kinetic parameters for experiments performed in the presence of BSA.

Identification of CYP Enzymes Mediating the Oxidative Metabolism of OLZ

The capacity of recombinantly expressed CYP 1A1, 1A2, 2B6, 2C8, 2C9, 2E1 and 3A4 to form oxidative metabolites of OLZ was assessed at OLZ concentrations of 50 and 300 μM. At the higher concentration of OLZ (Figure 3), *N*-desmethyl- and 2-hydroxymethyl-OLZ were formed to the greatest extent by rCYP2C8 (730 and 60 pmol/min/nmol P450, respectively), while 7-hydroxy-OLZ was formed mainly by rCYP1A2 (130 pmol/min/nmol P450). In addition, rCYP 1A2, 2B6, 2C9 and 3A4 formed 2-hydroxymethyl-OLZ, albeit to a lesser extent (< 50 pmol/min/nmol P450). OLZ-*N*-oxide was primarily formed by FMO3 (483 pmol/min/mg; data not shown) with minor contributions by CYP 2C8 and 3A4 (200 and 120 pmol/min/nmol P450, respectively).

Kinetics of OLZ Oxidative Metabolism by HLMs and rCYPs

Four oxidative metabolites formed by incubations of OLZ with HLMs, were identified by UPLC-MS. These were 2-hydroxymethyl-OLZ, 7-hydroxy-OLZ, *N*-desmethyl-OLZ and OLZ-*N*-oxide (retention times of 1.7, 2.2, 3.4 and 3.8 min, respectively; Figure 2, peaks 4 - 7). The kinetics of OLZ-*N*-demethylation and OLZ-7-hydroxylation were best described by the Michaelis-Menten equation, whereas OLZ-2-hydroxylation exhibited negative cooperativity (n ranging from 0.6 to 0.9). OLZ-*N*-oxide formation followed Michaelis-Menten kinetics in four out of five livers, with while in the remaining liver (H12) the formation of this metabolite was best described by the Hill equation (positive cooperativity, n = 1.5). Kinetic parameters for oxidative OLZ metabolism by HLMs are summarized in Table 2 and Eadie-Hofstee plots are shown in Figure 4 (panels A – C).

Kinetic parameters for the formation of the oxidative metabolites of OLZ by rCYP enzymes over the substrate concentration range of 5 – 1000 μM are shown in Table 3 and the Eadie-Hofstee plots are shown in Figure 4 (panels D – F). OLZ-*N*-demethylation by rCYP1A2 was best described by the Michaelis-Menten equation, while rCYP1A2 catalyzed OLZ-7-hydroxylation was best described by the Hill equation (negative cooperativity, n = 0.7). Kinetic data for OLZ-*N*-demethylation by rCYP2C8 was best described by the Michaelis-Menten equation.

Identification of UGT Enzymes Mediating the Glucuronidation of OLZ

The capacity of human UGT 1A1, 1A3, 1A4, 1A6, 1A7, 1A8, 1A9, 1A10, 2B4, 2B7, 2B10, 2B15 and 2B17 to catalyze the glucuronidation of OLZ was evaluated at substrate concentrations of 350 and 1500 μM. Only UGT1A4 converted OLZ to OLZ-10-*N*-glucuronide and OLZ-4′-*N*-glucuronide (Figure 2; peaks 1 - 3). This result differs from a previous *in vitro* study, which demonstrated that when overexpressed in HEK293 cells at an unusually high final incubation concentration of 30mg/mL, UGT2B10 glucuronidated OLZ, with intrinsic clearances for OLZ-10-*N*-glucuronide and OLZ-4′-*N*-glucuronide of 5 and 7 nL/min/mg, respectively (Erickson-Ridout et al., 2011). Screening experiments in the current study using Supersome expressed UGT2B10 (1 mg/mL; 2 h incubation) demonstrated no activity. Thus, subsequent kinetic studies were performed only with rUGT1A4.

OLZ Glucuronidation by HLMs and rUGT1A4

Previous studies characterizing OLZ metabolism *in vitro* have demonstrated the formation of three compounds with m/z consistent with that of OLZ-*N*-glucuronides (489.18). These compounds have been identified as two isomers of OLZ-10-*N*-glucuronide (Figure 2; peaks 1 and 2) and OLZ-4′-*N*-glucuronide (Figure 2; peak 3) (Kassahun et al., 1998; Erickson-Ridout et al., 2011). In the current study, limited formation of the OLZ-4′-*N*-glucuronide (<5% that of OLZ-10-*N*-glucuronide) was only detected in incubations performed at an increased HLM concentration of 1 mg/mL (a positive control for screening of UGT activities). As such, no kinetic analysis was performed to characterize the formation of this metabolite. Due to the lack of commercial availability of an authentic OLZ-10-*N*-glucuronide standard, chromatographic peaks were assigned to OLZ-10-*N*-glucuronide on the basis of mass spectral characteristics. OLZ-10-*N*-glucuronide was characterized by [M-H^+] peaks at m/z 313.16 (following the loss of the glucuronic moiety; molecular weight = 176 g/mol) and m/z 432.15 (following the loss of a methyl piperazine (CH_2=CH-NH-CH_3) moiety; molecular weight = 57 g/mol). The fragmentation pattern observed for OLZ-10-*N*-glucuronide was consistent with previous reports for this compound (Kassahun et al., 1998; Erickson-Ridout et al., 2011). Representative kinetic plots for OLZ-10-N-glucuronide formation by HLMs (liver H40), in the absence and presence of BSA, are

shown in Figure 5 (panel A) and mean kinetic parameters are summarized in Table 4. OLZ-10-*N*-glucuronidation by HLMs in the absence and presence of BSA were best described by the substrate inhibition equation. In the absence of BSA, the (mean ± SD) K_m and V_{max} values for OLZ 10-N-glucuronidation by HLMs were 634 ± 287 µM and 443 ± 176 pmol/min/mg, respectively. The addition of BSA did not alter kinetic parameters for HLM catalysed OLZ 10-N-glucuronidation (K_m 511 ± 245 µM, V_{max} 484 ± 170 pmol/min/mg), although substantial inter-liver variability was observed and may have masked any small effect. For experiments performed with recombinant UGT1A4, where variability is limited to experimental error, the addition of BSA decreased the K_m for OLZ 10-*N*-glucuronidation from 341 µM to 183 µM, with minor effects on V_{max} and K_{si}.

As observed in previous studies and incubations performed with HLMs, rUGT1A4 generated three chromatographic peaks identified as two isomers of OLZ-10-*N*-glucuronide and OLZ-4′-*N*-glucuronide. However, the low rate of OLZ-4′-*N*-glucuronide formation precluded kinetic analysis. As found with HLMs, experimental data for rUGT1A4 were best described by the substrate inhibition equation (Table 3). An Eadie-Hofstee plot for rCYP1A4 catalysed OLZ glucuronidation is shown in Figure 5 (panel B). K_m and V_{max} values for OLZ-10-*N*-glucuronidation by rUGT1A4 were lower than those for OLZ-10-*N*-glucuronidation by HLMs by 36 to 64%.

Inhibition Studies in Pooled HLMs

The effects of CYP3cide, diethyldithiocarbamic acid, furafylline, hecogenin, montelukast, quinidine, sulfaphenazole, ticlopidine and tranylcypromine on the formation of OLZ oxidation products by pooled HLMs were determined. The formation of *N*-desmethyl-OLZ was inhibited by 56, 27 and 35% by furafylline, montelukast and CYP3cide, respectively. The formation of 7-hydroxy-OLZ was markedly inhibited (84%) by furafylline whereas the effects of other CYP enzyme selective inhibitors were minor (<20% inhibition), except for CYP3cide which inhibited the formation of 7-hydroxy-OLZ by 24%.

The formation of 2-hydroxymethyl-OLZ was inhibited by furafylline, tranylcypromine, montelukast and CYP3cide by approximately 20 – 30%. CYP3cide also inhibited OLZ-*N*-oxide formation to a moderate extent (27%), whereas other CYP enzyme selective inhibitors had no effect on the formation of this metabolite. Tranylcypromine, ticlopidine, sulfaphenazole, diethyldithiocarbamate and quinidine had only a minor (<20% inhibition) or no effect on the formation of the OLZ oxidative metabolites. Human liver microsomal OLZ-10-*N*-glucuronide formation was inhibited >80% by hecogenin.

Discussion

This study reports for the first time, the major involvement of additional CYP enzymes, most notably CYP2C8, in OLZ-*N*-demethylation. This finding is of considerable clinical importance given the strong correlations between plasma *N*-desmethyl-OLZ concentration, clinical response to OLZ and the occurrence of adverse effects (Hägg et al., 2001; Carrillo et al., 2003; Shirley et al., 2003, Nozawa et al., 2008, Laika et al., 2010, Ghotbi et al., 2010, Skogh et al., 2011, Söderberg et al., 2013a). Variability in CYP2C8 protein expression and catalytic activity is well documented (Sonnichsen et al., 1995, Baldwin et al., 1999, Totah and Rettie, 2005, Naraharisetti et al., 2010). It is likely that the contribution of CYP2C8 and other CYP enzymes to *N*-desmethyl-OLZ formation may explain the poor correlation between CYP1A2 phenotype or genotype and plasma concentration of this metabolite (Hägg et al., 2001; Carrillo et al., 2003; Shirley et al., 2003). Indeed, given the comparable involvement of multiple enzymes in the formation of this metabolite, it is unlikely that consideration of any single metabolic pathway will provide a robust predictive marker of clinical outcomes with OLZ, and that a more complex model accounting for multiple covariates is required.

The sole previous study considering the CYP enzymes responsible for OLZ metabolism demonstrated that OLZ-*N*-demethylation is primarily catalyzed by CYP1A2, with minor contributions from CYP3A4 and CYP2D6 (Ring et al., 1996). FMO3 was reported to be the primary enzyme involved in the formation of OLZ-*N*-oxide, with minor contributions from CYP 1A2, 2D6, 2C9, 2E1 and 3A4 (Ring et al., 1996). However, the initial reaction phenotyping for OLZ oxidative metabolism was assigned on the basis of correlations of the rate of OLZ metabolite formation with immunoquantified CYP (1A2, 2A6, 2C9, 2C19, 2D6, 2E1 and 3A) and FMO3 levels in HLMs and (where possible), with the catalytic activity of form-selective probe substrates for these enzymes. Notably, confirmation of enzyme involvement using cDNA expressed enzymes was only reported for a limited panel of enzymes (CYP 1A2, 2A6, 2C9, 2D6, 2E1 and 3A4). Ring et al. (1996) did postulate the possible involvement of CYP2C8 in the formation of OLZ metabolites on the basis of correlation of the rates of OLZ metabolite formation with immunoquantified level of this enzyme. However, the significance of the role of CYP2C8 in terms of OLZ metabolite formation was excluded on the basis of poor

correlations; correlation coefficients (r) ranged from 0.19 for 2-hydroxymethyl-OLZ formation to 0.40 for *N*-desmethyl-OLZ formation. The approach used to assess the immunoquantified level of CYP was not reported by Ring et al. (1996). However, given the significant similarities in amino acid sequence within the CYP2C family (2C8, 2C9 and 2C19), it is plausible that antibody cross-reactivity may have confounded this result. Additionally, it should be noted that while correlations of the rate of *N*-desmethyl-OLZ formation with catalytic activities for CYP1A2 mediated ethoxyresorufin-*O*-deethylase and caffeine-3-demethylase (form-selective catalytic activities), were significant with r values of 0.64 and 0.66, respectively, correlation of the rate of *N*-desmethyl-OLZ formation with immunoquantified level of microsomal CYP1A2 (r = 0.35) was not significant, and in fact was poorer than the correlation observed for the immunoquantified level of CYP2C8. Due to the lack of a selective CYP2C8 probe at the time of the previous study, correlation of the rate of OLZ metabolite formation with a form-selective catalytic activity for CYP2C8 was not undertaken (Ring et al., 1996). In the current study, OLZ-*N*-demethylation by recombinant CYP 2C8 and 1A2 were the major oxidative pathways; scaling of kinetic data for relative liver CYP abundance demonstrate that these enzymes account for 28 and 26% of the total *in vitro* metabolism of OLZ, respectively. The role of FMO3 in the oxidative metabolism of OLZ (primarily OLZ-*N*-oxide formation) was confirmed. However, given the limited role of OLZ-*N*-oxide in determining OLZ plasma concentration and clinical outcomes (Söderberg et al., 2013b), and the recent in vitro characterization of this pathway (Cashman et al., 2008), subsequent kinetic studies were not performed.

Previous *in vitro* studies found that OLZ-10-*N*-glucuronide is formed by both UGT1A4 (Linnet, 2002) and UGT2B10 (Erickson-Ridout et al., 2011); the latter enzyme was also reported to be primarily responsible for the formation of OLZ-4′-*N*-glucuronide (a minor metabolite). However, the catalytic activity of rUGT2B10 was approximately 28-fold lower than that of rUGT1A4. Given the comparable levels of mRNA expression of UGT1A4 and UGT2B10 in human liver (1110 and 1004 copies per 10^9 copies of 18S rRNA, respectively) (Court et al., 2012), it is likely that the activity of UGT1A4 is more important in determining the formation of OLZ-*N*-glucuronides *in vivo*. Consistent with this finding, UGT1A4 was observed to be the major enzyme involved in OLZ-10-*N*-glucuronide

and OLZ-4′-*N*-glucuronide formation. These data are similarly consistent with the report of Kato et al. (2013), where despite referring to OLZ as a UGT2B10 substrate, the observed activity for UGT2B10 was less than 5% that of UGT1A4 and was too low to facilitate kinetic analysis. In the current study, the low rate of OLZ-4′-*N*-glucuronide formation by rUGT1A4 similarly precluded kinetic analysis of this pathway; this observation is also consistent with the previously reported low intrinsic clearance for UGT1A4-mediated OLZ-4′-*N*-glucuronidation of 10 ± 4 nL/min/μg (Erickson-Ridout et al., 2011). In contrast to the previous study, UGT2B10 did not catalyze OLZ-*N*-glucuronidation. Notably, the previously reported capacity of UGT2B10 to catalyze OLZ-*N*-glucuronidation was only observed in an experiment performed at an unusually high recombinant enzyme concentration of 30 mg/mL (Erickson-Ridout et al., 2011). Consistent with the major role of UGT1A4 in the formation of OLZ-10-*N*-glucuronides, inhibition experiments with hecogenin demonstrated > 80% inhibition of OLZ-10-*N*-glucuronide formation.

It has been demonstrated that endogenous long-chain unsaturated fatty acids, such as arachidonic acid, linoleic acid and oleic acid, are released from biological membranes during *in vitro* incubations (Rowland et al., 2008) and can inhibit the catalytic activities of multiple CYP and UGT enzymes, including CYP1A2, CYP2C8 and UGT1A4 (Rowland et al., 2006; Wattanachai et al., 2011 and 2012). This artefact of *in vitro* kinetic experiments typically manifests as a decrease in 'apparent' enzyme affinity (increase in K_m) for the added substrate and subsequent under-prediction of enzyme activity for the affected pathway. Inclusion of BSA in incubation samples restores the catalytic activity of affected enzymes by sequestering these fatty acids, thereby preventing their interaction with drug metabolizing enzymes (Rowland et al., 2008a). A concentration effect relationship for albumin has been demonstrated; an added BSA concentration of 0.5% (5mg/mL) causes a consistent >80% maximal decrease in K_m, while addition of 2% BSA (20mg/mL) has been demonstrated to cause a maximal decrease in K_m across multiple drug metabolizing enzymes. Notably, addition of BSA at a concentration <0.5% (most commonly 0.1%) has been associated with substantial variability in effect. In the current study, HLMs, *E.coli* membranes expressing rCYP and HEK293T cells

expressing rUGT were used as enzyme sources in kinetic experiments. Given the major roles of CYP1A2, CYP2C8 and UGT1A4 in the formation of OLZ metabolites, and limited binding of OLZ to BSA, kinetic parameters where determined in the presence of BSA (2%). Consistent with the effect of BSA the activity of these enzymes, the kinetics of OLZ metabolism demonstrated greater affinity (lower K_m) compared to previous findings (Ring et al., 1996). As the 'albumin effect' has been demonstrated for both CYP1A2 and CYP2C8 (Wattanachai et al. 2011 and 2012), studies were not performed in the absence of BSA for these enzymes. In contrast given the comparatively limited data concerning the effect of BSA on UGT1A4, studies with this enzyme were performed in the presence and absence of BSA (2%).

In conclusion, this study demonstrates that multiple CYP enzymes are involved in the metabolism of OLZ, particularly with regard to the formation of *N*-desmethyl-OLZ. This is a critical finding given the importance of *N*-desmethyl-OLZ as a marker of clinical response and adverse effects associated with the administration of OLZ. Indeed, data presented here raise the possibility that inter- and intra-individual variability in the activities of CYP 2C8 and 3A4 may additionally contribute to the therapeutic efficacy and tolerability of OLZ in humans.

Acknowledgments

Assistance from Dr Benjamin Lewis with rCYP enzyme expression is gratefully acknowledged, as are contributions from Dr Vidya Perera and Professor Jason Roberts to the conception of the study and its design.

Authorship Contributions

Participated in research design: Korprasertthaworn, McLachlan, Polasek, Miners, and Rowland

Conducted experiments: Korprasertthaworn and Rowland

Performed data analysis: Korprasertthaworn, Miners, and Rowland

Wrote or contributed to the writing of the manuscript: Korprasertthaworn, McLachlan, Polasek, Miners, Sorich, Tucker, and Rowland

References

Baldwin SJ, Clarke SE, and Chenery RJ (1999) Characterization of the cytochrome P450 enzymes involved in the in vitro metabolism of rosiglitazone. *Br J Clin Pharmacol* **48**: 424-432.

Baumann P, Hiemke C, Ulrich S, Eckermann G, Gaertner I, Gerlach M, Kuss HJ, Laux G, Müller-Oerlinghausen B, Rao ML, Riederer P, and Zernig G (2004) The AGNP-TDM expert group consensus guidelines: therapeutic drug monitoring in psychiatry. *Pharmacopsychiatry* **37**: 243-265.

Boase S and Miners JO (2002) *In vitro-in vivo* correlations for drugs eliminated by glucuronidation: investigations with the model substrate zidovudine. *Br J Clin Pharmacol* **54**: 493-503.

Bowalgaha K, Elliot DJ, Mackenzie PI, Knights KM, Swedmark S, and Miners JO (2005) S-Naproxen and desmethylnaproxen glucuronidation by human liver microsomes and recombinant human UDP-glucuronosyltransferases (UGT): role of UGT2B7 in the elimination of naproxen. *Br J Clin Pharmacol* **60**: 423-433.

Boye SL, Kerdpin O, Elliot DJ, Miners JO, Kelly L, Mckinnon RA, Bhasker CR, Yoovathaworn K, and Birkett DJ (2004) Optimizing bacterial expression of catalytically active human cytochromes P450: comparison of CYP2C8 and CYP2C9. *Xenobiotica* **34**: 49-60.

Callaghan JT, Bergstrom RF, Ptak LR, and Beasley CM (1999) Olanzapine: pharmacokinetic and pharmacodynamic profile. *Clin Pharmacokinet* **37**: 177-193.

Carrillo JA, Herráiz AG, Ramos SI, Gervasini G, Vizcaíno S, and Benítez J (2003) Role of the smoking-induced cytochrome P450 (CYP)1A2 and polymorphic CYP2D6 in steady-state concentration of olanzapine. *J Clin Psychopharmacol* **23**: 119-127.

Cashman JR, Zhang J, Nelson MR, and Braun A (2008) Analysis of flavin-containing monooxygenase 3 genotype data in populations administered the anti-schizophrenia agent olanzapine. *Drug Metab Lett* **2**: 100-114.

Court MH, Zhang X, Ding X, Yee KK, Hesse1 LM, and Finel M (2012) Quantitative distribution of mRNAs encoding the 19 human UDP-glucuronosyltransferase enzymes in 26 adult and 3 fetal tissues. *Xenobiotica* **42**: 266–277.

Erickson-Ridout KK, Zhu J, and Lazarus P (2011) Olanzapine metabolism and the significance of UGT1A4^{48V} and UGT2B10^{67Y} variants. *Pharmacogenet Genomics* **21**: 539-551.

Ghotbi R, Mannheimer B, Aklillu E, Suda A, Bertilsson L, Eliasson E, and Ösby U (2010) Carriers of the *UGT1A4* 142T>G gene variant are predisposed to reduced olanzapine exposure—an impact similar to male gender or smoking in schizophrenic patients. *Eur J Clin Pharmacol* **66**: 465-474.

Hägg SH, Spigset OS, Lakso HL, and Dahlqvist RD (2001) Olanzapine disposition in humans is unrelated to CYP1A2 and CYP2D6 phenotypes. *Eur J Clin Pharmacol* **57**: 493-497.

Kassahun K, Mattiuz E, Franklin R, and Gillespie T (1998) Olanzapine 10-*N*-glucuronide. A tertiary *N*-glucuronide unique to humans. *Drug Metab Dispos* **26**: 848-855.

Kassahun K, Mattiuz E, Nyhart E, Obermeyer B, Gillespie TA, Murphy AT, Goodwin R, Tupper DE, Callaghan JT, and Lemberger L (1997) Disposition and biotransformation of the antipsychotic agent olanzapine in humans. *Drug Metab Dispos* **25**: 81-93.

Kato Y, Izukawa T, Oda S, Fukami T, Finel M, Yokoi T, Nakajima M (2013) Human UDP glucuronosyltransferase (UGT) 2B10 in drug *N*-glucuronidation: Substrate screening and comparison with UGT1A3 and UGT1A4. *Drug Metab Dispos* **41:** 1389-1397

Laika B, Leucht S, Heres S, Schneider H, and Steimer W (2010) Pharmacogenetics and olanzapine treatment: *CYP1A2*1F* and serotonergic polymorphisms influence therapeutic outcome. *Pharmacogenomics J* **10**: 20-29.

Linnet K (2002) Glucuronidation of olanzapine by cDNA-expressed human UDP-glucuronosyltransferases and human liver microsomes. *Hum Psychopharmacol* **17**: 233-238.

Mauri MC, Volonteri LS, Colasanti A, Fiorentini A, De Gaspari IF, and Bareggi SR (2007) Clinical pharmacokinetics of atypical antipsychotics: a critical review of the relationship between plasma concentrations and clinical response. *Clin Pharmacokinet* **46**: 359-388.

McLure JA, Miners JO, and Birkett DJ (2000) Nonspecific binding of drugs to human liver microsomes. *Br J Clin Pharmacol* **49**: 453-461.

Miners JO and Mackenzie PI (1991) Drug glucuronidation in humans. *Pharmacol Ther* **51**: 347-369.

Naraharisetti SB, Lin YS, Rieder MJ, Marciante KD, Psaty BM, Thummel KE, and Totah RA (2010) Human liver expression of CYP2C8: gender, age, and genotype effects. *Drug Metab Dispos* **38**: 889-893.

Nozawa M, Ohnuma T, Matsubara Y, Sakai Y, Hatano T, Hanzawa R, Shibata N, and Arai H (2008) The relationship between the response of clinical symptoms and plasma olanzapine concentration, based on pharmacogenetics: Juntendo University Schizophrenia Projects (JUSP). *Ther Drug Monit* **30**: 35-40.

Perry PJ, Lund BC, Sanger T, and Beasley C (2001) Olanzapine plasma concentrations and clinical response: acute phase results of the North American olanzapine trial. *J Clin Psychopharmacol* **21**: 14-20.

Ring BJ, Catlow J, Lindsay TJ, Gillespie TA, Roskos LK, Cerimele BJ, Swanson SP, Hamman MA, and Wrighton SA (1996) Identification of the human cytochromes P450 responsible for the *in vitro* formation of the major oxidative metabolites of the antipsychotic agent olanzapine. *J Pharmacol Exp Ther* **276**: 658-666.

Rosenheck R, Perlick D, and Bingham S (2003) Effectiveness and cost of olanzapine and haloperidol in the treatment of schizophrenia: a randomized controlled trial. *JAMA* **290**: 2693-2702.

Rowland A, Elliot DJ, Williams JA, Mackenzie PI, Dickinson RG, and Miners JO (2006) In vitro characterization of lamotrigine *N*2-glucuronidation and the lamotrigine-valproic acid interaction. *Drug Metab Dispos* **34**: 1055-1062.

Rowland A, Gaganis P, Elliot DJ, Mackenzie PI, Knights KM, and Miners JO (2007) Binding of inhibitory fatty acids is responsible for the enhancement of UDP-glucuronosyltransferase 2B7 activity by albumin: implications for in vitro-in vivo extrapolation. *J Pharmacol Exp Ther* **321**: 137-147.

Rowland A, Knights KM, Mackenzie PI, and Miners JO (2008a) The "albumin effect" and drug glucuronidation: bovine serum albumin and fatty acid-free human serum albumin enhance the glucuronidation of UDP-glucuronosyltransferase (UGT) 1A9 substrates but not UGT1A1 and UGT1A6 activities. *Drug Metab Dispos* **36**: 1056-1062.

Rowland A, Elliot DJ, Mackenzie PI, Knights KM, and Miners JO (2008b) The "albumin effect" and in vitro – in vivo extrapolation: Sequestration of long chain unsaturated fatty acids enhances phenytoin hydroxylation by human liver microsomal and recombinant cytochrome P450 2C9. *Drug Metab Dispos* **36**: 870-877.

Rowland A, Miners JO, and Mackenzie PI (2013) The UDP-glucuronosyltransferases: their role in drug metabolism and detoxification. *Int J Biochem Cell B* **45**: 1121-1132.

Schwenger E, Dumontet J, and Ensom MHH (2011) Does olanzapine warrant clinical pharmacokinetic monitoring in schizophrenia? *Clin Pharmacokinet* **50**: 415-428.

Shirley KL, Hon YY, Penzak SR, Lam YWF, Spratlin V, and Jann MW (2003) Correlation of cytochrome P450 (CYP) 1A2 activity using caffeine phenotyping and olanzapine disposition in healthy volunteers. *Neuropsychopharmacology* **28**: 961-966.

Skogh E, Sjödin I, Josefsson M, and Dahl ML (2011) High correlation between serum and cerebrospinal fluid olanzapine concentrations in patients with schizophrenia or schizoaffective disorder medicating with oral olanzapine as the only antipsychotic drug. *J Clin Psychopharmacol* **31**: 4-9.

Söderberg MM, Haslemo T, Molden E, and Dahl ML (2013a) Influence of CYP1A1/CYP1A2 and AHR polymorphisms on systemic olanzapine exposure. *Pharmacogenet Genomics* **23**: 279-285.

Söderberg MM, Haslemo T, Molden E, Dahl ML (2013b) Influence of *FMO1* and *3* polymorphisms on serum olanzapine and its N-oxide metabolite in psychiatric patients. *Pharmacogenomics J* **13**: 544-550.

Sonnichsen DS, Liu Q, Schuetz EG, Schuetz JD, Pappo A, and Relling MV (1995) Variability in human cytochrome P450 paclitaxel metabolism. *J Pharmacol Exp Ther* **275**: 566-575.

Totah RA and Rettie AE (2005) Cytochrome P450 2C8: substrates, inhibitors, pharmacogenetics, and clinical relevance. *Clin Pharmacol Ther* **77**: 341-352.

Tsoutsikos P, Miners JO, Stapleton A, Thomas A, Sallustio BC, and Knights KM (2004) Evidence that unsaturated fatty acids are potent inhibitors of renal UDP-glucuronosyltransferases (UGT):

kinetic studies using human kidney cortical microsomes and recombinant UGT1A9 and UGT2B7. *Biochem Pharmacol* **67**: 191-199.

Uchaipichat V, Mackenzie PI, Guo XH, Gardner-Stephen D, Galetin A, Houston JB, and Miners JO (2004) Human UDP-glucuronosyltransferases: enzyme selectivity and kinetics of 4-methylumbelliferone and 1-naphthol glucuronidation, effects of organic solvents, and inhibition by diclofenac and probenecid. *Drug Metab Dispos* **32**: 413-423.

Wattanachai N, Polasek T, Heath T, Uchaipichat V, Tassaneeyakul W, Tassaneeyakul W, and Miners JO (2011) In vitro–in vivo extrapolation of CYP2C8-catalyzed paclitaxel 6α-hydroxylation: effects of albumin on in vitro kinetic parameters and assessment of interindividual variability in predicted clearance. *Eur J Clin Pharmacol* **67**: 815-824.

Wattanachai N, Tassaneeyakul W, Rowland A, Elliot DJ, Bowalgaha K, Knights KM, and Miners JO (2012) Effect of albumin on human liver microsomal and recombinant CYP1A2 activities: impact on in vitro-in vivo extrapolation of drug clearance. *Drug Metab Dispos* **40**: 982-989.

Yao HT, Chang YW, Lan SJ, Chen CT, Hsu JTA, and Yeh TK (2006) The inhibitory effect of polyunsaturated fatty acids on human CYP enzymes. *Life Sci* **79**: 2432-2440.

Zanger UM, Schwab M (2013) Cytochrome P450 enzymes in drug metabolism: Regulation of gene expression, enzyme activities, and impact of genetic variation. *Pharmacol Ther* **138**: 103-141.

Footnote

This study was supported by the Simcyp Grant and Partnership Scheme, Simcyp Limited (a Certera company), Sheffield, United Kingdom.

Figure Legends

Figure 1. Schematic of OLZ metabolism investigated in *in vitro* by this study. A previous study identified OLZ-10-*N*-glucuronide as a major metabolite of OLZ in urine (Kassahun et al., 1997). Gluc, Glucuronide.

Figure 2. Extracted ion chromatograms for OLZ oxidative and glucuronide metabolites formed by HLM. The oxidation assay was performed using HLM (0.5 mg/mL) and 50 μM OLZ, while the glucuronidation assay contained HLM (1 mg/mL) and 1 mM OLZ. Both reactions were performed at 37°C for 1 h. (A) Peaks at m/z 489.18; (B) Peak at m/z 299.14 and (C) Peaks at m/z 329.15. Peak 1, OLZ-10-*N*-glucuronide isomer 1; peak 2, OLZ-10-*N*-glucuronide isomer 2; peak 3, OLZ-4′-*N*-glucuronide; peak 4, *N*-desmethyl-OLZ; peak 5, 2-hydroxymethyl-OLZ; peak 6, 7-hydroxy-OLZ; peak 7, OLZ-*N*-oxide.

Figure 3. *In vitro* formation of OLZ oxidative metabolites by *E. coli* expressed CYP. Formation of *N*-desmethyl-OLZ, 2-hydroxymethyl-OLZ, 7-hydroxy-OLZ and OLZ-*N*-oxide by rCYP enzymes (25 pmol P450/mL) incubated with 300 μM OLZ at 37°C for 2 h. Data are shown as the means of duplicate determinations from a single experiment.

Figure 4. Representative Eadie-Hofstee plots for OLZ oxidative metabolism. (A) OLZ-*N*-demethylation by HLM_H7; (B) OLZ-2-hydroxylation by HLM_H7; (C) OLZ-7-hydroxylation by HLM_H7; (D) OLZ-*N*-demethylation by rCYP1A2; (E) OLZ-*N*-demethylation by rCYP2C8; and (F) OLZ-7-hydroxylation by rCYP1A2, in the presence of BSA. Points are experimentally determined values (means of duplicate and quadruplicate measurements at each concentration for HLM_H7 and rCYP enzymes, respectively) while curves are from model-fitting.

Figure 5. Eadie-Hofstee plots for OLZ 10-*N*-glucuronidation. (A) OLZ 10-*N*-glucuronidation by HLM_H40 and (B) OLZ 10-*N*-glucuronidation by rUGT1A4, in the presence (▲) and absence (◇) of BSA. Points are experimentally determined values (means of quadruplicate measurements at each concentration); lines are model fits.

Tables

Table 1

Parameter	Setting
Capillary voltage (kV)	2.1
Sampling cone voltage (eV)	25
Extraction cone voltage (eV)	5.0
Source temperature (°C)	90
Desolvation temperature (°C)	270
Cone gas flow (L/hr)	50
Desolvation gas flow (L/hr)	550
Collision energy (eV)	3
Detector voltage (eV)	1750

DMD Fast Forward. Published on September 1, 2015 as DOI: 10.1124/dmd.115.064790
This article has not been copyedited and formatted. The final version may differ from this version.

Table 2 Derived kinetic parameters for OLZ oxidative pathways by HLMs in the presence of BSA (2% w/v).

Pathway	K_m or S_{50}	V_{max}
	(μM)	(pmol/min/mg)
***N*-demethylation**	22 ± 8	70 ± 15
7-hydroxylation	14 ± 3	33 ± 19
***N*-oxidation**[a]	228 ± 107	250 ± 70
2-hydroxylation[b]	638 ± 352	28 ± 11

Data are the mean ± S.D. for microsomes from 5 individual livers.

[a] Experimental data for one liver (H12) was best described by the Hill equation (n = 1.5).

[b] Kinetic constants from fitting with the Hill equation (n = 0.6 – 0.9).

DMD Fast Forward. Published on September 1, 2015 as DOI: 10.1124/dmd.115.064790
This article has not been copyedited and formatted. The final version may differ from this version.

Table 3 Derived kinetic parameters for OLZ oxidative metabolism by rCYP enzymes in the presence of BSA (2%w/v).

Enzyme / Pathway	K_m or S_{50}	V_{max}
	(μM)	(pmol/min/nmol P450)
***N*-demethylation**		
CYP1A2	61 ± 20	1340 ± 90
CYP2C8	30 ± 7	1370 ± 210
7-hydroxylation		
CYP1A2 [a]	592 ± 85	1921 ± 21

Data are mean ± S.D. from quadruplicate experiments.

[a] Kinetic constants from fitting with the Hill model, (n = 0.7).

DMD Fast Forward. Published on September 1, 2015 as DOI: 10.1124/dmd.115.064790
This article has not been copyedited and formatted. The final version may differ from this version.

Table 4 – Derived kinetic parameters for OLZ-10-*N*-glucuronidation by HLMs and rUGT1A4 in the absence and presence of albumin.

Enzyme	Without BSA			With 2% BSA		
	K_m	V_{max}	K_{si}	K_m	V_{max}	K_{si}
	(μM)	(pmol/min/mg)	(μM)	(μM)	(pmol/min/mg)	(μM)
HLMs [a]	634 ± 287	443 ± 176	1082 ± 409	511 ± 245	484 ± 170	869 ± 809
UGT1A4 [b]	341 ± 19	285 ± 10	1628 ± 131	183 ± 36	216 ± 14	1836 ± 54

[a] Data are mean ± S.D. from quadruplicate measurements for HLMs from each of 5 individual livers.

[b] Data are mean ± S.D. from quadruplicate measurements.

DMD Fast Forward. Published on September 1, 2015 as DOI: 10.1124/dmd.115.064790
This article has not been copyedited and formatted. The final version may differ from this version.

Figure 1

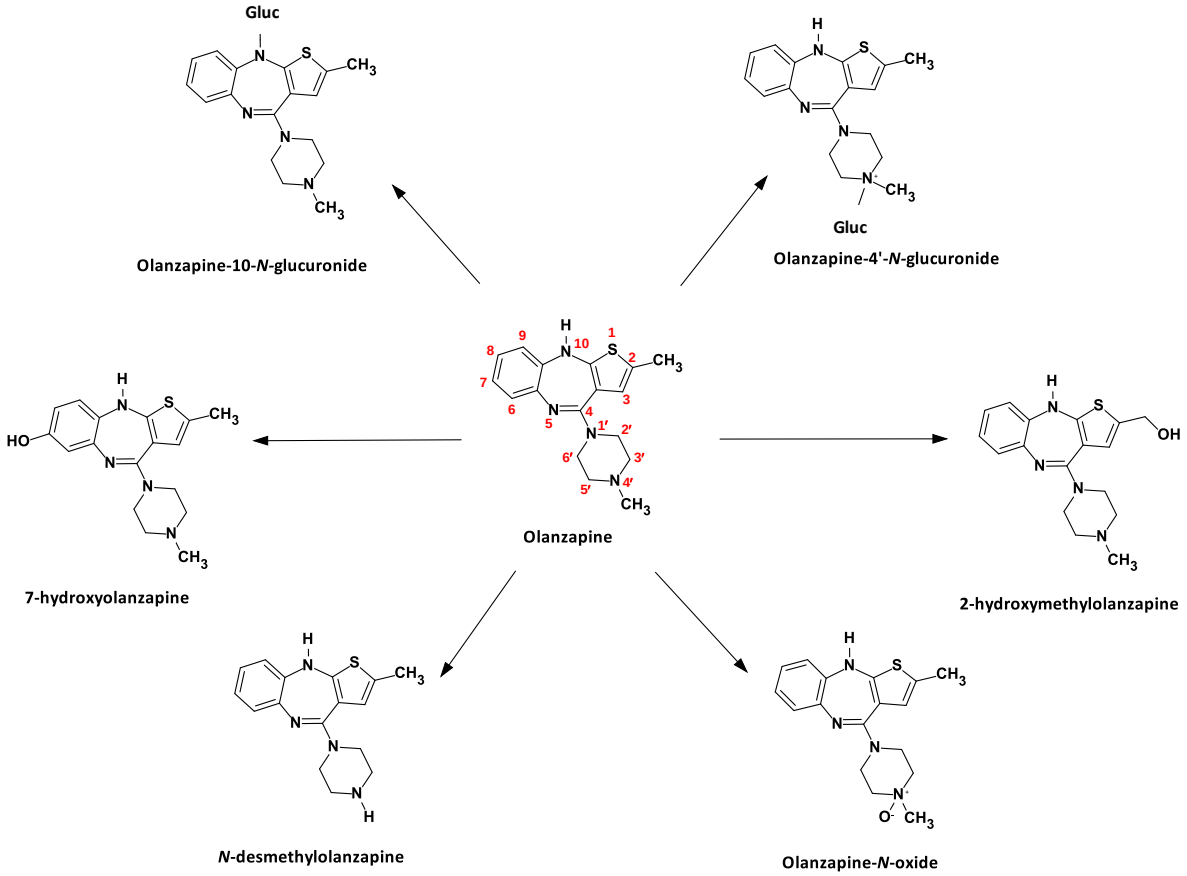

Figure 2

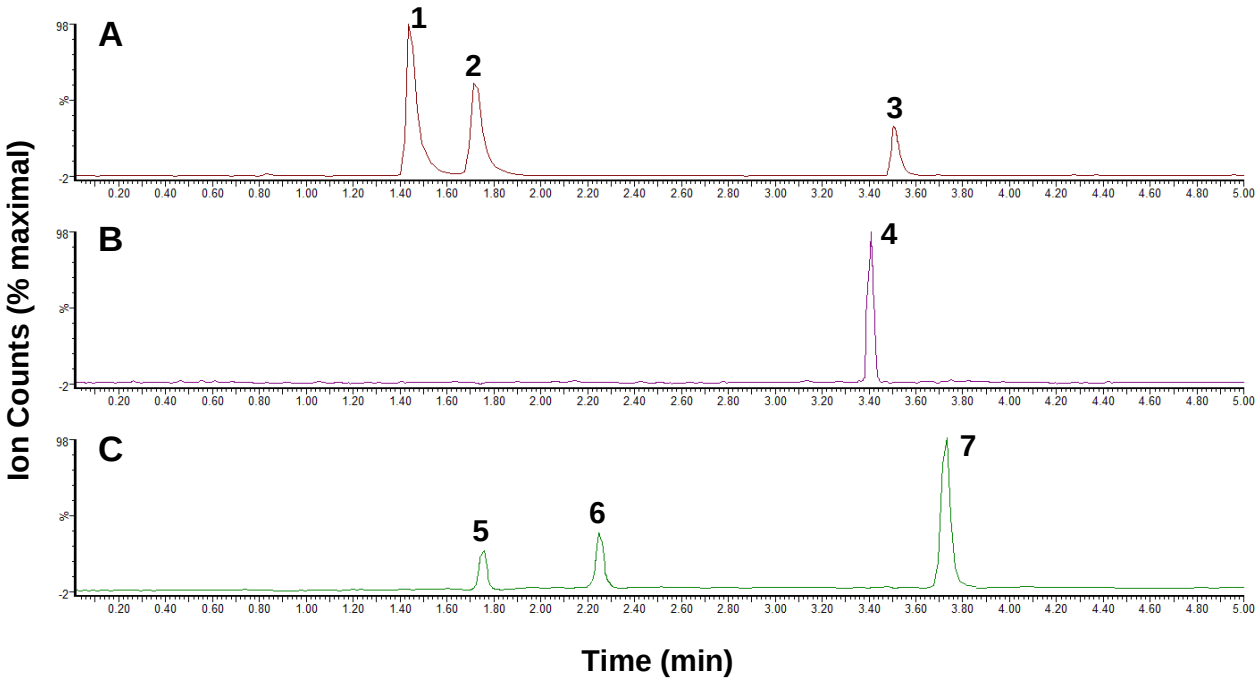

DMD Fast Forward. Published on September 1, 2015 as DOI: 10.1124/dmd.115.064790
This article has not been copyedited and formatted. The final version may differ from this version.

Figure 3

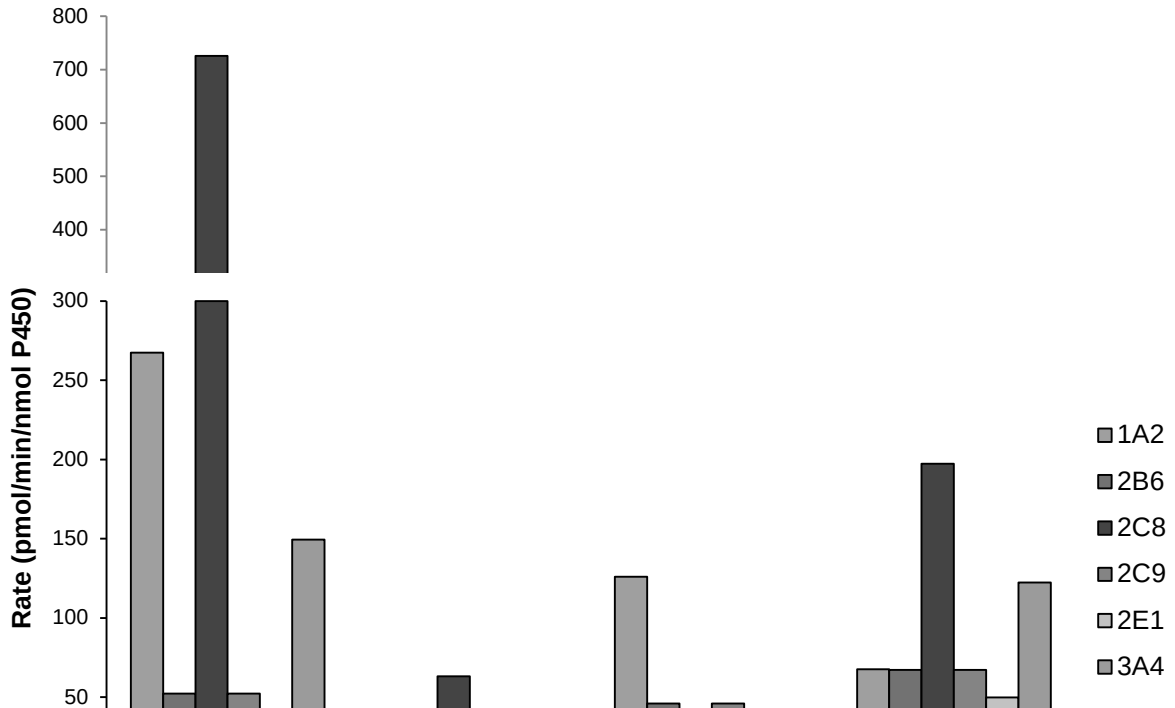

Figure 4

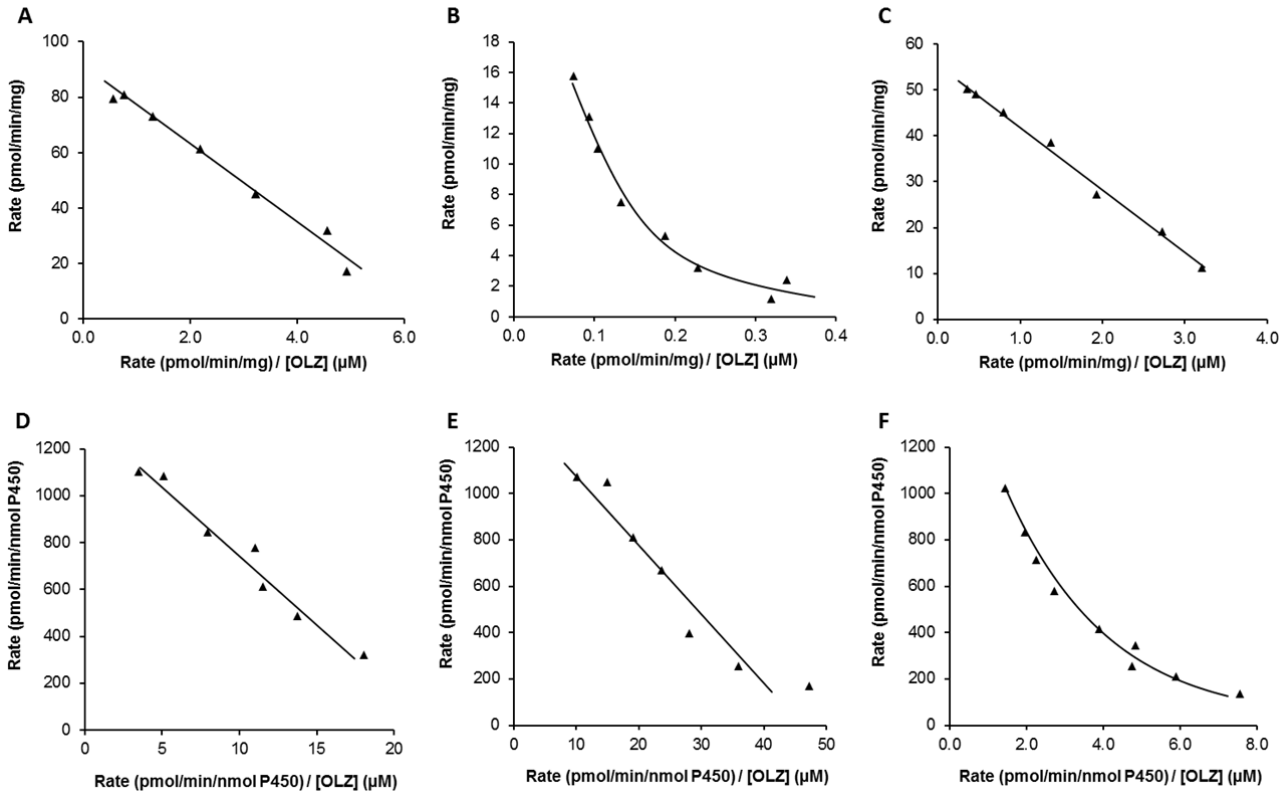

DMD Fast Forward. Published on September 1, 2015 as DOI: 10.1124/dmd.115.064790
This article has not been copyedited and formatted. The final version may differ from this version.

Figure 5